Research Article Vol. 32, No. 2 / 15 Jan 2024 / Optics Express 1562
Optics EXPRESS

$\mathcal{PT}$-symmetry breaking in dual-core phosphate-glass photonic crystal fibers

MATTIA LONGOBUCCO,[1,2,3,6,7] LE XUAN THE TAI,[4] VIET HUNG NGUYEN,[5] JAROSŁAW CIMEK,[1] BARTOSZ PAŁUBA,[2] RYSZARD BUCZYŃSKI,[1,2] AND MAREK TRIPPENBACH[2]

[1]*Department of Glass, Łukasiewicz Research Network - Institute of Microelectronics and Photonics, Aleja Lotników 32/46, 02-668 Warsaw, Poland*
[2]*Faculty of Physics, University of Warsaw, Pasteura 5, 02-093 Warsaw, Poland*
[3]*School of Electrical and Electronics Engineering, Nanyang Technological University, 50 Nanyang Avenue, 639798 Singapore, Singapore*
[4]*Faculty of Physics, Warsaw University of Technology, Koszykowa 75, 00-662 Warsaw, Poland*
[5]*International Training Institute for Materials Science (ITIMS), Hanoi University of Science and Technology (HUST), No. 1 - Dai Co Viet Str., Hanoi, Vietnam*
[6]*mattia.longobucco@imif.lukasiewicz.gov.pl*
[7]*mlongobucco@fuw.edu.pl*

Abstract: We investigate the properties of a soft glass dual-core photonic crystal fiber for application in multicore waveguiding with balanced gain and loss. Its base material is a phosphate glass in a P_2O_5-Al_2O_3-Yb_2O_3-BaO-ZnO-MgO-Na_2O oxide system. The separated gain and loss cores are realized with two cores with ytterbium and copper doping of the base phosphate glass. The ytterbium-doped core supports a laser (gain) activity under excitation with a pump at 1000 nm wavelength, while the CuO-doped is responsible for strong attenuation at the same wavelength. We establish conditions for an exact balance between gain and loss and investigate pulse propagation by solving a system of coupled generalized nonlinear Schrödinger equations. We predict two states of light under excitation with hyperbolic secant pulses centered at 1000 nm: 1) linear oscillation of the pulse energy between gain and loss core ($\mathcal{PT}$-symmetry state), with strong power attenuation; 2) retention of the pulse in the excited gain core (broken $\mathcal{PT}$-symmetry), with very modest attenuation. The optimal pulse energy levels were identified to be 100 pJ (first state) and 430 pJ (second state).

1. Introduction

$\mathcal{PT}$-symmetry is a theoretical concept elaborated by Bender et al. in 1998 [1]. It is based on the possibility of treating a Hermitian quantum system as a combination of two non-Hermitian non-isolated subsystems [2]. Both of them are characterized by a nonzero flux of probability, positive and negative respectively, across their boundaries; however, the non-isolated combined system has no net flux of probability, i.e. it could exhibit real spectra or equivalently real eigenvalues [3]. It was shown that the condition for $\mathcal{PT}$-symmetry is that the complex potential V involved satisfies the requirement $V(x) = V^*(-x)$. This concept finds application in several fields of science, such as atomic systems [4], mechanics [5] and electronics [6].

In the field of optics and the paraxial propagation regime, the condition on complex potential translates into the one on the real and imaginary part of the refractive index, which should be symmetric and anti-symmetric, respectively [7], i.e.

$$n(x, y) = n^*(-x, y) \tag{1}$$

#505927 https://doi.org/10.1364/OE.505927
Journal © 2024 Received 28 Sep 2023; revised 30 Nov 2023; accepted 8 Dec 2023; published 3 Jan 2024

Optics EXPRESS

This means that the two refractive index profiles should be symmetric with respect to the central symmetry point and should have the same absolute values [8,9] If this condition is not satisfied, the eigenvalues of the system cease to be real and the parity-time symmetry breaks down (it is referred as $\mathcal{PT}$-symmetry breaking), leading to complex spectra [10]. Theoretical works predicted such scenario in several optical systems [7,11,12], and also experimental verifications were achieved in periodic structures [13], photonics lattices [14], semiconductor-based dual microring laser resonators [15], plasmonic systems [16] and - recently - in high power large-area lasers [17].

One of the simplest realizations of $\mathcal{PT}$-symmetric optical system is a coupled waveguide, with one subjected to gain (active waveguide) and the other one to loss (dissipative waveguide) [18,19] Moreover, it is possible to benefit the optical properties of gain/loss waveguides even in the nonlinear regime, i.e. studying $\mathcal{PT}$-symmetry in nonlinear directional couplers [20]. In these systems, the non-Hermitian eigenvectors formally maintain the same structural form of the corresponding linear one [8,21,22] It has been demonstrated that such systems are beneficial for all-optical switching in the nonlinear regime because of the possibility to lower the required switching power [23], achieve faster transition [24] and support stable switching states due to the possibility to support solitons [25,26] The exact analytical formalism describing the switching dynamics in nonlinear $\mathcal{PT}$-symmetric couplers has been presented in [27]. In the last decades, dual-core [28,29] and multicore optical fibers [30], which are one of the possible implementations of the nonlinear directional coupler, have attracted significant interest in the implementation of nonlinear $\mathcal{PT}$-symmetric systems due to their possible application in all-optical signal processing. In particular, dual-core fibers (DCFs) consist of two parallel cores throughout their whole length: one of the cores should provide gain for the guided light along propagation (gain core), while the other one should cause losses to the propagating light (loss core). To satisfy Eq. (1), the amount of provided gain and loss should be equal.

In this manuscript we present a proof of concept, a possible implementation of a $\mathcal{PT}$-symmetric optical system in the form of a DC photonic crystal fiber (PCF). The crucial features of such systems are two regions of dynamics (stable and unstable) separated by the so-called exceptional point. It is the area around the exceptional point that seems to be the most interesting, and we can tune it by changing the system parameters, e.g. the intensity of the incident pulse.

The base material of the fiber is phosphate glass in a P_2O_5-Al_2O_3-Yb_2O_3-BaO-ZnO-MgO-Na_2O oxide system [31]. The gain and loss cores are implemented by ytterbium-based and copper-based doping, respectively. The fiber is suitable for fabrication by the stack-and-draw method [32]. We present the numerical studies of nonlinear phenomena in such $\mathcal{PT}$-symmetric optical systems, first evaluating the effective parameters and then showing the predictions of pulse propagation in such systems using a simple model. These considerations can also be seen as an interesting perspective for all-optical switching using fiber-based devices.

2. Materials and design

The implementation of $\mathcal{PT}$-symmetric DC PCF requires first of all the gain core. We propose to take advantage of the Yb-doped phosphate glass photonic crystal fiber laser fabricated by our group [33]. The core material is phosphate glass doped with 6% mol of Yb_2O_3 ($15.69 \cdot 10^{20}$ Yb^{3+} cm^{-3}). In the frame of this study, a laser generation is demonstrated at the central wavelength of approximately 1 µm with more than 400 dB $\cdot$ m^{-1} of pump absorption and the highest generation power of 150 W $\cdot$ m^{-1}. The pump is a laser diode with a wavelength of 973.5 nm and 3 nm bandwidth. The threshold power for laser activity is 8.7 W, while the maximum pump power could reach the value of 35 W. The maximum output laser power in the continous wave (CW) regime is 9 W. The slope efficiency, which indicates the power conversion between the pump and the laser beam – i.e. power pump/laser gain– could be as high as 36.2%. For our purpose, we consider this value as the target value of gain.

Optics EXPRESS

Next, we focus on the loss core. In order to respect the balance between gain and loss, we need to use in the loss core a glass that realizes a 36.2% power attenuation – or equivalently 63.8% transmission – at 1 μm and the same length of 6 cm. In order to estimate the loss coefficient for the loss core α, we use the standard Beer-Lambert law, $P(z) = P_0 e^{-\alpha z}$, where P_0 is the input power and z is the propagation distance. Considering that $P(z = 6\text{ cm})/P_0$ should be $\approx 63.8\%$, the absorption coefficient resulted in the value of $\alpha = 7.49\text{ m}^{-1}$. Here we propose CuO-doped glass for the loss core. As the phosphate glass has a much higher attenuation than silica (0.46 vs 0.001 m^{-1}) [31], the estimated required percentage of copper doping should be rather low, at the level of 0.015% CuO.

Figure 1(a) reports the refractive index profile of the phosphate glass (blue curve) and Yb-doped one (red curve) in the spectral range 430-1490 nm, while Fig. 1(b) shows the difference between the two refractive indices in the same spectral range. The difference between the refractive indices is rather low, reaching a maximum value of approximately $1.4 \cdot 10^{-3}$ at 1490 nm. At 1000 nm, the difference is $1.04 \cdot 10^{-3}$. The nonlinear refractive index n_2 of phosphate glass is $0.99 \cdot 10^{-19}\text{ m}^2 \cdot \text{W}^{-1}$ at 1064 nm [34], approximately 4 times higher than the fused silica one ($0.246 \cdot 10^{-19}\text{ m}^2 \cdot \text{W}^{-1}$ [35]).

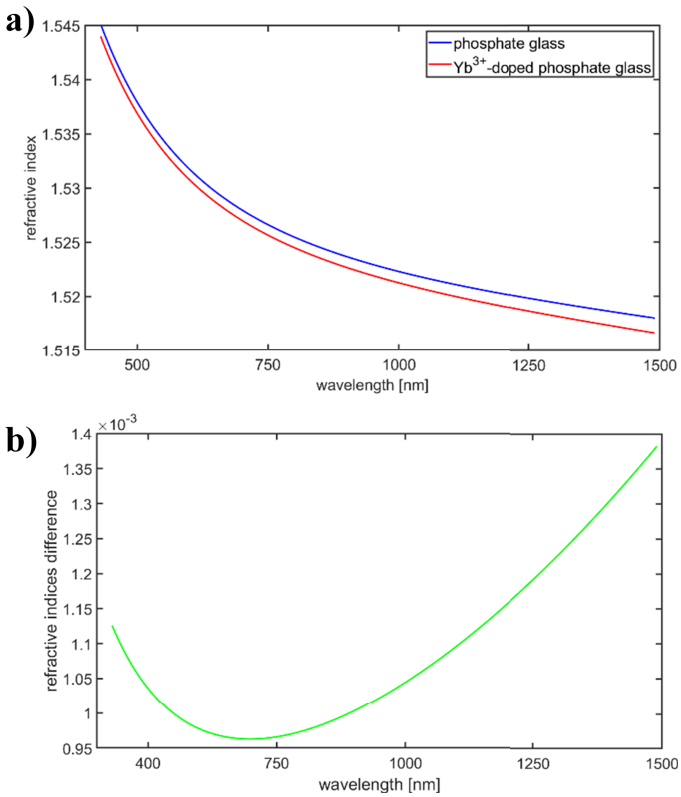

Fig. 1. (a) Refractive index profiles of the undoped phosphate glass (blue curve) and Yb-doped one (red curve) in the spectral range 430-1490 nm. (b) Difference of the refractive indices between undoped and Yb-doped phosphate glasses in the same spectral range.

3. Finding optical properties

For the particular design of the fiber (including geometry and the material), we can find the optical properties of the setup using numerical tools, for instant commercial *Lumerical* software.

Optics EXPRESS

We started with the design shown in Fig. 2(a) (schematic plot of the proposed fiber). This seemed to be a natural choice. Notice that due to the small refractive index difference between Yb-doped and undoped phosphate glass (see Fig. 1(b)), we need to introduce a photonic lattice of air holes in the undoped phosphate glass in order to support the fundamental modes and improve the coupling efficiency between the cores [36]. In a courteous manner, we would like to convey that as of now, no study or fabrication has been conducted on CuO-doped phosphate glass with such expected low doping (0.015%) in our institute. Consequently, to simulate the optical properties of such fiber-based $\mathcal{PT}$-symmetric system, we opted to replace the CuO-doped loss core with a ytterbium-doped one. This substitution is based on the anticipation of a very low concentration of CuO-doping (0.015% mol of CuO compared to 6% mol of Yb_2O_3 for loss and gain cores, respectively) and the expected minimal difference in refractive indices between CuO-doped and undoped phosphate glass, similarly as reported in Fig. 1 between Yb-doped and undoped phosphate glass. Therefore, further studies are required to get more experience with CuO-doped phosphate glass. Hence, at the moment, we limit our investigation to a PCF with two Yb-doped phosphate glass, as reported in Fig. 2(b), where the gain core has a negative absorption coefficient value ($\alpha = -7.49$ m^{-1}), and the loss core a positive one ($\alpha = 7.49$ m^{-1}), in order to preserve $\mathcal{PT}$-symmetry [1,3]. The comprehensive study of the complete PT-symmetric fiber-based system proposed in Fig. 2(a) will be deferred until we conduct thorough theoretical and experimental examinations of CuO-doped phosphate glass.

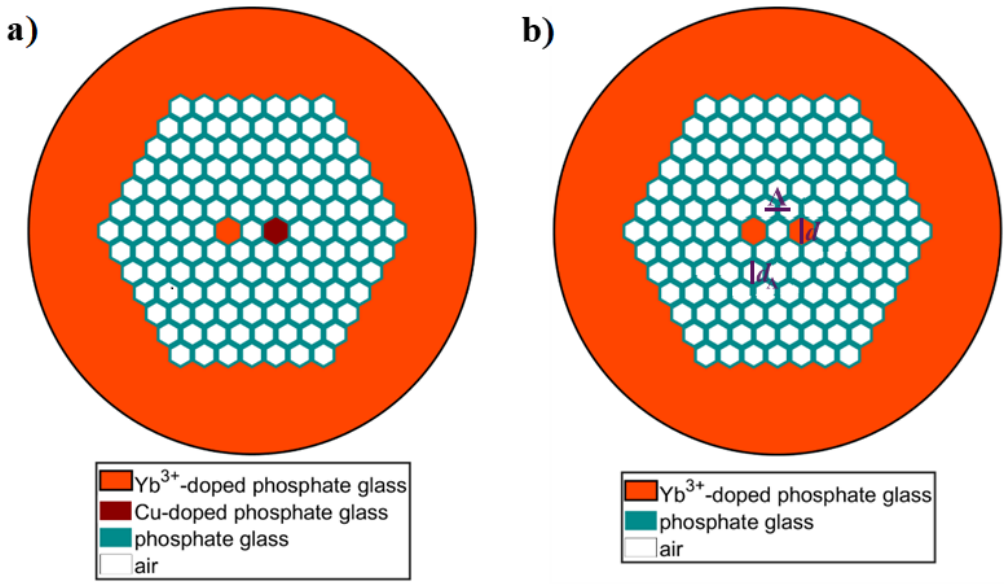

Fig. 2. (a) Structure of the designed DC PCF laser: Yb-doped phosphate glass for the gain core, Cu-doped one for the loss core, and undoped phosphate glass for the cladding. An extra photonic lattice of air holes is introduced to support the coupling between the cores. (b) Fiber structure used for the simulation phase: the material of the loss core has been substituted from Cu-doped phosphate glass to Yb-doped phosphate glass.

Here we consider the structure in Fig. 2(b), where we replace the Cu-doped core with another Yb-doped one. The cores diameter d (same for both cores) and the lattice pitch Λ (marked with violet lines in Fig. 2(b)) were the same as the optimized soft glass DCF presented in [37]. We used the same structure with $d = 1.85$ µm and $\Lambda = 1.6$ µm and added an extra photonic lattice of air holes with diameter $d_A = 1.4$ µm surrounding the two Yb-doped cores. The distance between centers of the cores is then $2\Lambda = 3.2$ µm, as in the fiber structure in [38].

Optics EXPRESS

Subsequently, the new structure was characterized in the context of optical field propagation in the linear regime. The commercial Mode Solution software from *Lumerical* was used to calculate the spectral dependences of the field mode profile, the corresponding effective index, and the waveguide losses for each fundamental mode. All the relevant quantities were acquired in the spectral window between 500 and 2400 nm, which sufficiently covers the wavelength of our interest (1000 nm).

Figure 3 shows the dispersion profiles of the fundamental supermodes, with horizontal polarization direction (along X-axis) and dual-core symmetric state. The dispersion is normal (D<0) in the wavelength range of 800-1200 nm. We calculated another important linear parameter, the coupling length L_c. From the theory of nonlinear directional couplers, we know that, in the DCFs, the input radiation coupled in one of the two cores experiences (in the linear regime) periodic oscillations between cores with a period equal to L_c, defined as

$$L_c = \frac{\pi}{|\beta_S - \beta_A|}, \tag{2}$$

where β_S and β_A are the propagation constants of symmetric and antisymmetric supermodes of the fiber, respectively [38,39].

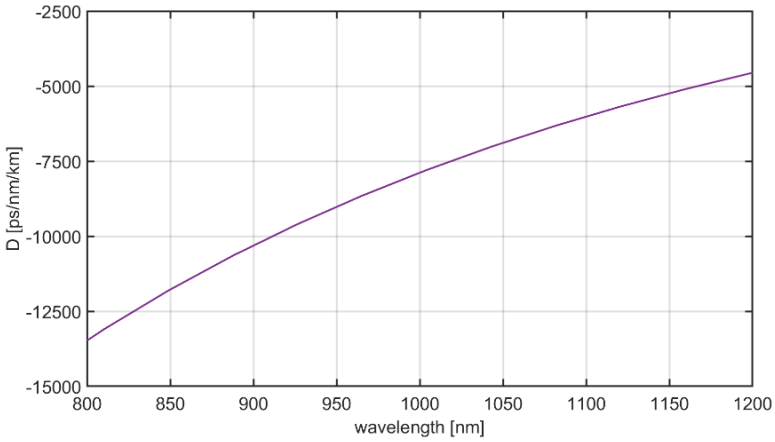

Fig. 3. Simulated dispersion curves of the fundamental Symmetric-X supermode of the dual-core structure in Fig. 2(b). The fiber shows normal dispersion in the whole range of 800-1200 nm.

Figure 4 reports the coupling length characteristics of the two fundamental supermodes, with horizontal and vertical polarization direction (X- and Y-polarization, respectively) in the same wavelength range of Fig. 3 (800-1200 nm). At 1000 nm, the values of L_c are 4.7 and 7.3 cm, respectively.

We calculated other linear and nonlinear parameters at the wavelength of interest i.e. 1000 nm, which were used for the numerical simulations. They include the effective refractive indices of the cores n_{eff}, the propagation constants β_0, β_1, β_2, the coupling coefficient κ and the nonlinear parameter γ. All the values except κ were calculated for a single core structure, that was obtained by filling one of the cores with undoped phosphate glass with diameter d = 1.85 µm and including one air hole with diameter d_A = 1.4 µm. We calculate the dispersion profile of the single-core fibers (left and right core separately) using Mode Solution software from *Lumerical*, including also the spectral dependences of the field mode profile, the corresponding effective index, and the waveguide losses for each fundamental mode. We also calculated the coupling coefficient κ between the two single-core modes based on the overlap integrals [39].

Optics EXPRESS

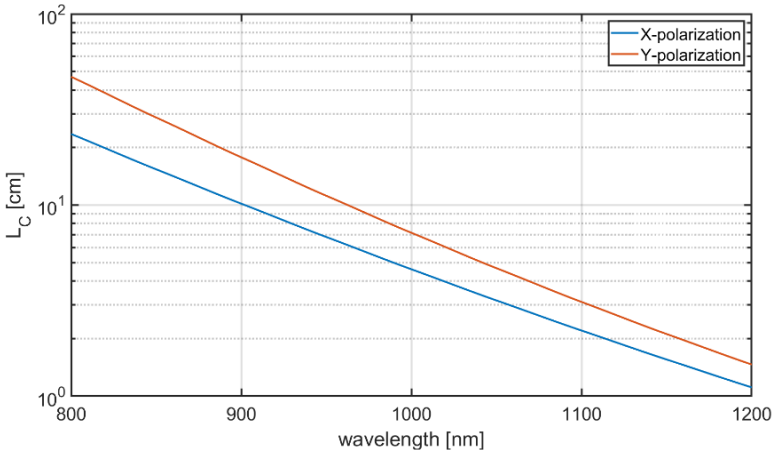

Fig. 4. Simulated coupling length L_c spectral characteristics for fundamental X- and Y-polarized modes of the DC PCF in Fig. 2(b). The values are calculated using Eq. (2).

4. Numerical simulations of pulse propagation: method and results

In this section, we develop numerical methods to study the $\mathcal{PT}$-symmetric dynamics in our system. The goal of this part of the investigation is twofold. First, we identify the most important parameters (eliminating the others) and then we study the role of chromatic dispersion of the crucial characteristics: pulse dispersion, inter-core coupling, and gain/loss coefficient.

4.1. Generalized Nonlinear Schrodinger Equation

In order to have a complete view of the system dynamics, the coupled generalized nonlinear Schrödinger equations (CGNSE) were solved numerically, including effects like coupling coefficient dispersion, self-steepening nonlinearity, and its spectral dependence, stimulated Raman contribution, cross-phase modulation, and waveguide losses. The resulting mathematical model is a system of two equations expressed in the following set of equations ($r = 1, 2$)

$$\begin{aligned}\frac{\partial A_{(r)}(z,t)}{\partial z} &= (-1)^{r+1}\left(-i\delta_0 A_{(r)}(z,t) - \delta_1\frac{\partial A_{(r)}(z,t)}{\partial t}\right) + \sum_l \frac{i^l}{l!}\alpha_l^{(r)}\frac{\partial^l A_{(r)}(z,t)}{\partial t^l} + \\ &+ \frac{1}{2}\sum_m \frac{i^{m+1}}{m!}\beta_m^{(r)}\frac{\partial^m A_{(r)}(z,t)}{\partial t^m} + \sum_n \frac{i^{n+1}}{n!}\kappa_n^{(r)}\frac{\partial^n A_{(3-r)}(z,t)}{\partial t^n} + \\ &+ i\gamma^{(r)}\left[\left(1 + i\tau_{shk}^{(r)}\frac{\partial}{\partial t}\right)\int_{-\infty}^{\infty} R(\tau)\left|A_{(r)}(z,t-\tau)\right|^2 d\tau + \sigma^{(r)}|A_{(3-r)}(z,t)|^2\right]A_{(r)}(z,t)\end{aligned} \tag{3}$$

where $r = 1, 2$ denotes the number of the core (1 – gain core, 2 – loss core), A_r is the corresponding electric field amplitude and quantities $\delta_0 = (\beta_0^{(r)} - \beta_0^{(3-r)})$ and $\delta_1 = (\beta_1^{(r)} - \beta_1^{(3-r)})$ represent the difference between the phase and group velocities respectively. Furthermore, $\alpha_k^{(r)}$, $\beta_k^{(r)}$ and $\kappa_k^{(r)}$ are the k-th order of Taylor expansion coefficients around the central frequency of gain/loss coefficient, propagation constant (dispersion) and coupling coefficient, respectively. Finally, $\gamma^{(r)}$ is the nonlinear parameter, $\tau_{shk}^{(r)}$ is the characteristic time of shock wave formation, R is the Raman response function and $\sigma^{(r)}$ is the overlap integral between the single core modes defining for the cross-phase modulation effect in the r-th core. Both experimentally determined instantaneous Kerr and delayed Raman response of the guiding PBG-08 glass are included in the material nonlinear response function.

Optics EXPRESS

To solve the equation, we used the single core fiber parameters and the identified coupling coefficients retrieved from *Lumerical* and presented in the previous section. Moreover, we introduced the gain and loss coefficient in the CGNLSE by modeling the function of the loss coefficient $\alpha^{(r)}(\lambda)$. We modeled $\alpha^{(r)}(\lambda)$ to have a Gaussian-like profile in the wavelength domain as follows:

$$\alpha^{(r)}(\lambda) = (-1)^r \alpha_p \cdot \exp\left[\frac{(\lambda - \lambda_0)^2}{2\sigma_\lambda^2}\right], \tag{4}$$

where $\lambda_0 = 1000$ nm, which corresponds to the frequency $\omega_0 = \frac{2\pi c}{\lambda_0} = 1.8837 \cdot 10^{15}$ rad $\cdot$ s^{-1}, $\sigma_\lambda = 100$ nm is the standard deviation of the Gaussian and $\alpha_p = 7.49$ m^{-1} is the peak amplitude. The α coefficient profile for the gain core closely aligns with the experimental data presented in [33]. In contrast, the profile for the loss core is artificially modelled. It exhibits a positive peak $\alpha_p = 7.49$ m^{-1}, along with identical σ_λ and λ_0. Due to unavailability of fabricated CuO-doped glass in our institute at the time of this study, we set the copper doping at 0.015% and estimated, through simulation, that the glass should exhibit a similar profile to the Yb-doped glass, albeit with a positive sign. As explained in the previous section, this is in accordance with the $\mathcal{PT}$-symmetric theory, where gain and loss should be balanced [1,3].

The CGNLSE in Eq. (3) was solved numerically by the Split-Step Fourier method with 160,000 steps [38]. After every 400 calculation steps, the field arrays were saved and then used to plot the output propagation maps; this means that the whole propagation distance is divided into 400 intervals. This approach represents a good compromise between the calculation time and the resolution of the propagation distance (fiber length). It is also the most common practice and the simplest approach for simulations of ultrashort optical pulse dynamics in PCFs. We considered a fiber length of 30 cm, which is 10 times larger than the estimated coupling length at 1000 nm (see Fig. 4). Using the Split-Step method, we considered the whole spectral behavior of loss and gain and applied them always at the frequency step. The input pulse shape was approximated by the sech^2 function, which is a good approximation for ultrafast oscillators. The power envelope of the pulse is expressed as:

$$P(t) = \frac{0.88E}{T_{FWHM}} \mathrm{sech}^2\left(\frac{1.763t}{T_{FWHM}}\right) \tag{5}$$

At each of the 400 propagation steps, we integrated the pulse envelopes in each core to observe the trend of the energy transfer along propagation. Figure 5 shows the propagation maps in case of 1000 nm wavelength, 1 ps pulse width hyperbolic secant pulse excitation with energy 100 pJ (top row) and 430 pJ (bottom row). We selected these energies by looking at several propagation maps and corresponding dynamics of the normalized integrated energies, and estimated that the $\mathcal{PT}$-symmetry breaking occurs at around 400 pJ. At 430 pJ, an energy increase through the fiber length is predicted in the gain core, with some low-input features after 20 cm.

4.2. Simplified theoretical model

To simplify the model in Eq. (3), we set $\sigma = 0$ (no cross-phase modulation), $t_{shk} = 0$ (no shock wave formation), and $\int_{-\infty}^{\infty} R(\tau)d\tau = 1$ (impulsive Raman response). Moreover, we limited the dispersion terms to the second-order $\beta_2^{(r)}$, and only linear coupling. Due to the sensitivity of the system towards the change of gain and loss, we keep the gain/loss coefficient with the full spectral dependence. We considered symmetric fiber structure, therefore $\kappa_0^{(1,2)} = \kappa_0^{(2,1)} = \kappa_0$, $\beta_2^{(1)} = \beta_2^{(2)} = \beta_2$ and $\gamma^{(1)} = \gamma^{(2)} = \gamma$. Set of Eqs. (3) takes the form as follows

$$\frac{\partial A_{(r)}(z,t)}{\partial z} = -\frac{i\beta_2}{2}\frac{\partial^2 A_{(r)}(z,t)}{dt^2} + i\kappa_0 A_{(3-r)}(z,t) + \left(\widetilde{\alpha^{(r)}} * A_{(r)}\right)(z,t) + i\gamma \left|A_{(r)}(z,t)\right|^2 A_{(r)}(z,t) \tag{6}$$

Optics EXPRESS

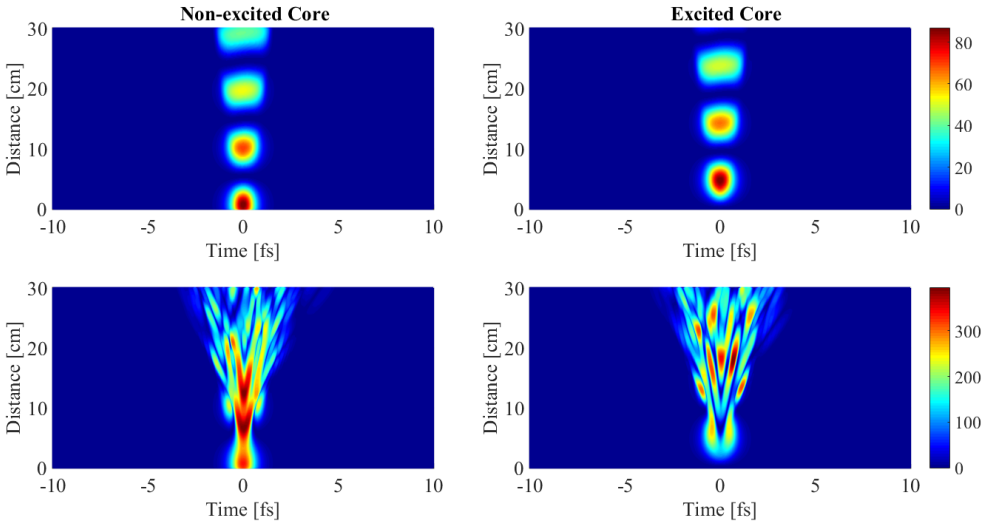

Fig. 5. Time domain evolution of the field intensity in the excited (left) and non-excited (right) core under excitation by 1000 nm central wavelength and 1 ps width pulses with 100 pJ (top) and 430 pJ (bottom) energies, in the case of gain core (left) excitation of a 30 cm length fiber with structure as in Fig. 2(b).

where $(r = 1, 2)$. Since the function $\alpha^{(r)}$ is defined in the frequency domain $(\alpha^{(r)} = \alpha^{(r)}(\omega))$ it is crucial to apply convolution according to the following property of Fourier transform: $\widetilde{(f \cdot g)}(t) = (\tilde{f} * \tilde{g})(t)$. In our case, it is given by: $(\widetilde{\alpha^{(r)} \cdot \tilde{A}_{(r)}})(z, t) = (\widetilde{\alpha^{(r)}} * A_{(r)})(z, t)$.

For the simulation study with the simplified model, we used the optical parameters calculated at 1000 nm central wavelength by *Lumerical*. All the parameters are the same for both cores. The estimated value for the gain/loss coefficients (7.49 m^{-1}) was included in the parameter α_0: it has a positive sign for loss, indicating power attenuation, and negative one for gain, indicating power increase. The other parameters were $\beta_2 = 4.21 \times 10^{-25}$ m · s^{-2}, $\gamma = 0.3$ $W^{-1} \cdot m^{-1}$ and $\kappa_0 = 33.74$ m^{-1}.

We generated, with our simplified model, 2D time-domain evolution plots with parameters corresponding to those used in Fig. 5 and the difference was hard to notice. Therefore, in order to trace subtle differences we looked at the pulse shapes in the time domain at 4 specific fiber lengths for the two cases above. The result is shown in Fig. 6 for input energies 100 pJ and 430 pJ, respectively. Solid lines present the results of the simulation obtained using the full model (red: unexcited, loss core; blue: excited, gain core), while dashed lines present the ones obtained using the simplified model. We clearly see the effect of dispersion, as pulse broadening in time. The small difference at the rising edge is due to the higher order nonlinearity associated with the parameter τ_{shk}, responsible for the shock wave formation. In Fig. 7, we compare pulse shapes generated by both methods; the four panels refer to lengths: (a) 8 cm, (b) 12 cm, (c) 21 cm, and (d) 30 cm. We observed that there is a close correspondence between the two models in each reported case. A small discrepancy between the models is observed only on the rising edge of the pulse in the loss core at 21 and 30 cm (i.e. between solid and dashed red lines of Fig. 7(c) and (d) for t in the range -1.0 to 1.0). In Fig. 8, which was calculated in the unstable regime, the four panels refer to lengths: (a) 8 cm, (b) 10 cm, (c) 12 cm and (d) 14 cm. In this case, as observed in Fig. 8(c) and (d), the two models give significantly different results after 12 cm and 14 cm. The solid and dashed curves differ much more from each other than in case of 8 cm and 10 cm of propagation distances. It is not a surprise that in an unstable regime, propagation is

Optics EXPRESS

sensitive to the fiber parameters used in the extended and simplified models, which becomes more visible with increasing propagation distance. However, the good news is, that the position of the exceptional point, the border between stable and unstable regimes, in both models is very similar. Hence, the simplified model can be used for finding critical intensity in the nonlinear regime.

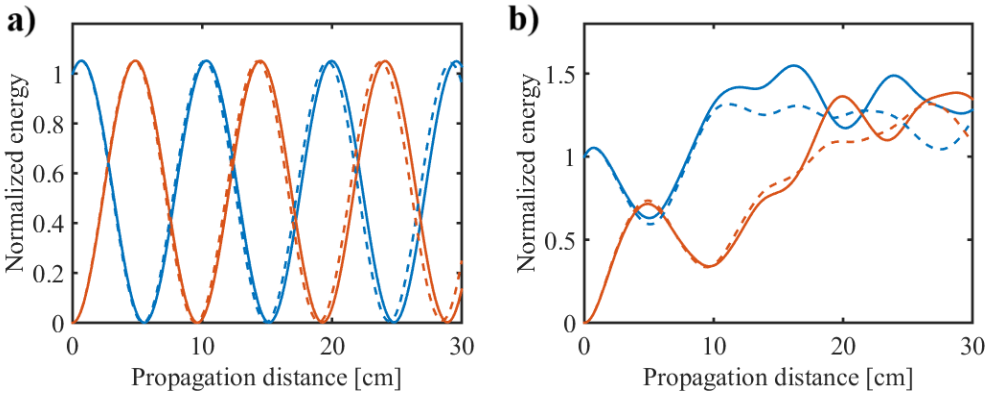

Fig. 6. Normalized integrated energies in the corresponding cores at the corresponding energy levels of (a) 100 pJ and (b) 430 pJ for full (solid blue lines: gain core, solid red lines: loss core) and simplified model (dashed blue lines: gain core, dashed red lines: loss core).

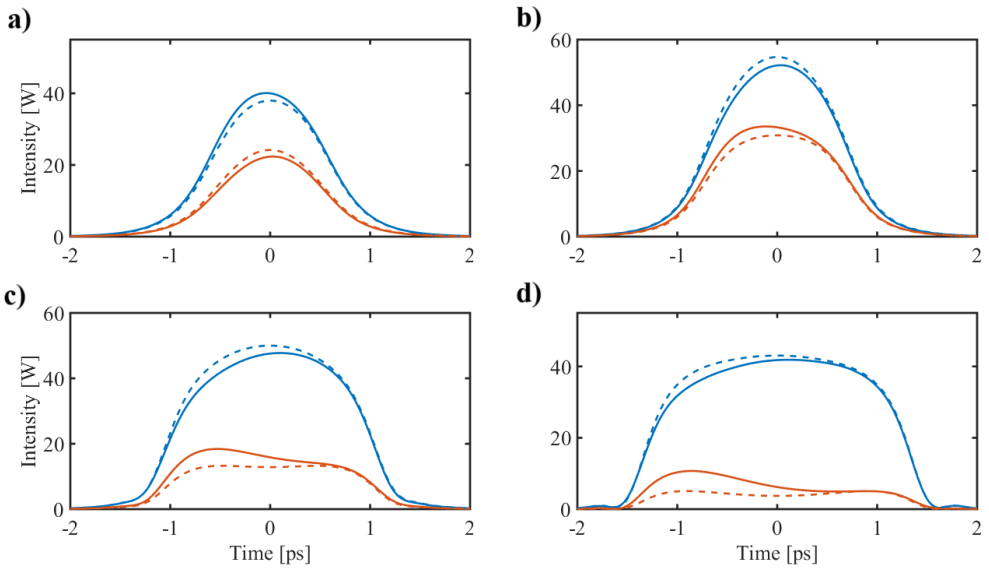

Fig. 7. Snapshot of 100pJ pulses corresponding cores simulated in full model (solid blue lines: gain core, solid red lines: gain core) and simplified model (dashed blue lines: gain core, dashed red lines: loss core) at different propagation distances: a) 8 cm, b) 12 cm, c) 21 cm and d) 30 cm.

4.3. Role of dispersion

In this section, we investigate the role of the dispersion on the stability of pulse propagation in a waveguide with two coupled cores: inter-core coupling κ and gain/loss coefficient α. We

Optics EXPRESS

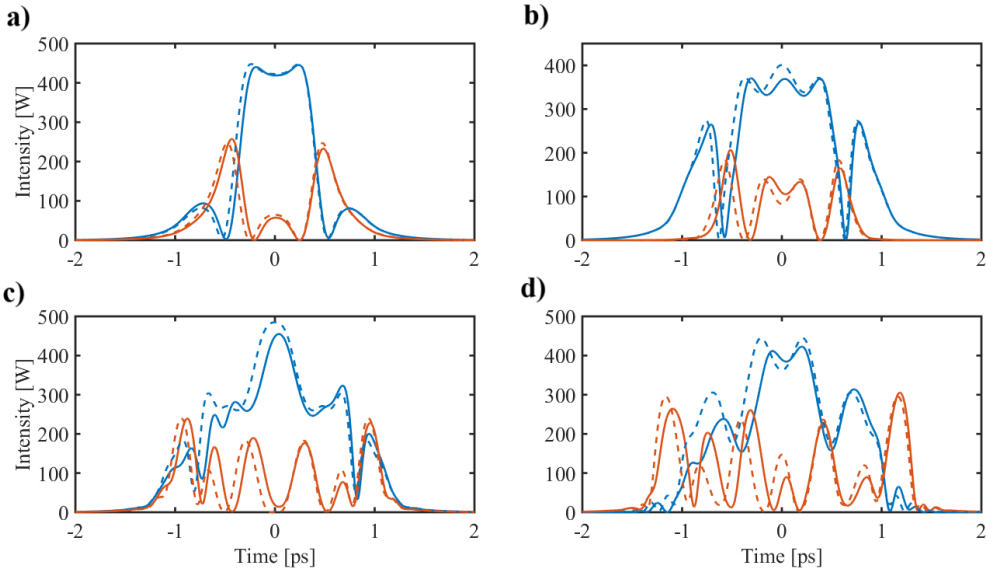

Fig. 8. Snapshot of 430 pJ pulses corresponding cores simulated in full model (solid blue lines-gain core, solid red lines-gain core) and simplified model (dashed blue lines: gain core, dashed red lines: loss core) at different propagation distances: a) 8 cm, b) 10 cm, c) 12 cm and d) 14 cm.

emphasize this aspect because, upon analyzing the outcomes of the simplified model, it stands out as the most dominant phenomenon, primarily due to its association with the shapes of absorption profiles. We restrict the analysis to the linear regime and study the dynamics described by the equation

$$\frac{\partial A_{(r)}(z,t)}{\partial z} = -\frac{i\beta_2}{2}\frac{\partial^2 A_{(r)}(z,t)}{\partial t^2} + i\left(\widetilde{\kappa} * A_{(3-r)}\right)(z,t) + \left(\widetilde{\alpha} * A_{(r)}\right)(z,t). \tag{7}$$

Note that we have two terms on the right hand side of the Eq. (7) in the form of a convolution. Each of the functions κ and α depend on the frequency ω. For the current study, we have chosen Gaussian functions for all dispersion profiles and each of them is characterized by three parameters: width σ, central frequency ω_0 and maximums κ_0 and α_0 respectively. For example, the inter-core coupling function will be defined as

$$\kappa(\omega) = \kappa_0 \exp\left[\frac{(\omega-\omega_{0,\kappa})^2}{\sigma_\kappa^2}\right]. \tag{8}$$

The dispersion in the gain/loss coefficient $\alpha(\omega)$ is introduced by analogy. We have checked that our conclusions are the same if we use Lorenzian functions instead of Gaussians in the frequency domain. In this formulation, the constant coefficient corresponds to the Gaussian function, which is a very broad function of frequency (formally for $\sigma \to \infty$). In each of the studies reported below, we looked for the exceptional point that lies on the boundary between stable and unstable propagation regions. Unstable propagation is characterized by the exponential growth of the signal in the gain core, while in the lossy core the pulse decays rapidly to zero.

In the case of linear propagation considered here, it is sufficient to examine the maximal real part of the eigenvalue $\Re(\lambda)_{max}$ of the characteristic equation derived from Eq. (7). It is worth noting, that this result remains consistent regardless of the shape of intensity of the input pulse. In the nonlinear scenario, however, our approach becomes ineffective. Then, in order to predict the dynamics of the system and to identify the specific exceptional points, we must resort to

Optics EXPRESS

direct simulations. The ability to find these exceptional points depends on various parameters associated with the cores, and this requires a different methodology compared to the linear case.

First, we considered the case where all coefficients are constant. In this case, the system becomes unstable when the magnitude of α is greater than the inter-core coupling κ, regardless of the value of the dispersion β_2, which is a well-known result. Then, we introduced the dispersion to κ and α in the manner described above. A summary of this study is shown in Fig. 9. We clearly observed that, as long as the width of the coupling σ_κ is greater than the gain/loss profile given by σ_α, we have a region of stable dynamics (while the maximums $\kappa_0 > \alpha_0$). In the opposite case, when the width of the gain/loss function exceeds the width of the coupling function, $\Re(\lambda)_{max}$ is always positive and tends to linear growth (with increasing value of α_0) as the gain/loss profiles become more and more narrow. This gives us a clue about the possible components of our system. If we include a small nonlinearity, we expect essentially the same characteristics, with the shift of the exceptional point.

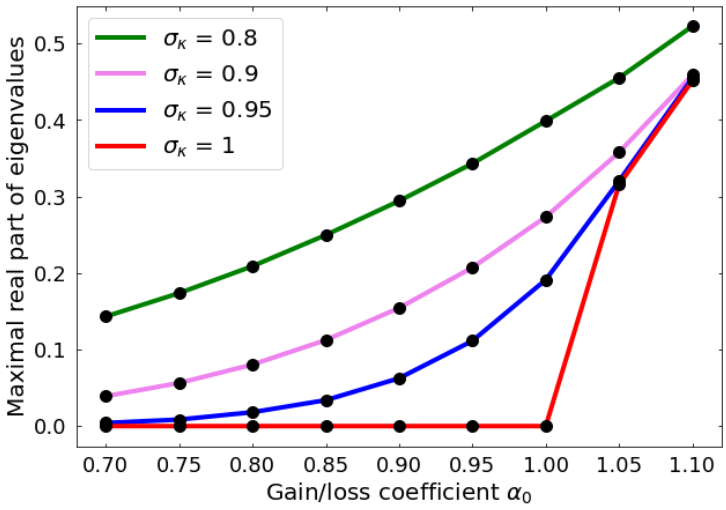

Fig. 9. Maximum value of the real part of the eigenvalues for different amplitudes of the coupling coefficient. The width of the gain/loss coefficient is arbitrarily set equal to one, and the widths of the coupling coefficients as a function of ω are given in the inset. Note that in all cases where the width of the coupling is smaller than the width of the gain/loss coefficient, we do not observe stable propagation.

Finally, we investigated, whether the center frequency for the gain/loss and coupling profiles need not be the same. To do this, we introduced the shift $\Delta = |\omega_{0,\alpha} - \omega_{0,\kappa}|$ between the two profiles and set the width of the inter-core coupling to be several times greater than the width of the gain/loss parameter ($\sigma_\kappa = 6$ and $\sigma_\alpha = 1$). As it can be seen in Fig. 10, as long as the shift between the two profiles is smaller than the width of the coupling (note that we arbitrarily choose the value of the gain/loss profile to be equal to one), an exceptional point appears. We have carried out thorough studies, including various coupling widths and shifts, to establish that the features shown in Fig. 10 are representative over a wide range of parameters, including proposed configuration. Although, our conclusion is purely qualitative, it serves the purpose of our pilot study. The main insight from our simulations is that, for practical implementation, we should look for setups with consistent coupling and carefully study how the relative shifts of the resonances, in both κ and α coefficients, vary with frequency.

Optics EXPRESS

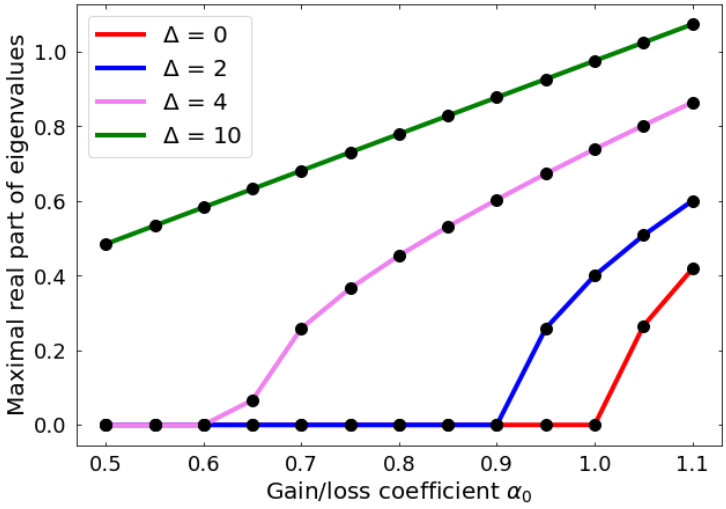

Fig. 10. Maximal real part from the set of eigenvalues in the case when gain/loss and inter-core coefficients are centered at frequencies shifted by Δ, as indicated in the inset. Other parameters are: $\beta_2 = 4$, $\sigma_\alpha = 1$, $\sigma_\kappa = 6$ and $\kappa_0 = 1$.

5. Conclusion

We predicted $\mathcal{PT}$-symmetry breaking in a DC PCF made of phosphate glasses synthesized in-house. The fiber cores are made of phosphate glasses with 6% mol of Yb_2O_3 (gain core) and 0.015% mol CuO doping (loss cores) and have the following structural parameters: core diameters of 1.85 µm, lattice pitch of 1.6 µm, and extra photonic lattice of air holes with diameter of 1.4 µm. The fiber exhibits normal dispersion of the fundamental supermodes in the range of 500-2000 nm and coupling length in the order of 5 cm at 1000 nm. We investigated the stability of the $\mathcal{PT}$-symmetric DC PCF system by simulating the propagation of hyperbolic secant pulses with a width of 10 ps and 1 ps: the system is stable considering both temporal widths and values of gain/loss and coupling coefficients ratio being $\alpha/\kappa \leq 0.25$. The designed fiber resulted in a α/κ value of 0.22. Then, we solved the system of CGNLSE with the Split-Step method, considering excitation pulses with a wavelength of 1000 nm and width of 1 ps. We predicted two regimes of light propagation through the designed fiber: 1) linear oscillations of the pulse energy between the gain and loss core ($\mathcal{PT}$-symmetry state); 2) unstable dynamics with strong enhancement in both cores (broken $\mathcal{PT}$-symmetry). Initial input energies were 100 pJ and 430 pJ, respectively. The same scenarios were predicted considering pulses with the same input energy and using a simplified theoretical model, which only includes second-order dispersion term, linear coupling, first-order nonlinearity, and dispersive gain/loss coefficient. We carried out an extensive investigation of the influence of dispersion on both the gain/loss and the coupling. Our investigation led us to understand that stable dynamics prevails when the coupling width (σ_κ) exceeds the gain/loss profile width ($\sigma_\kappa > \sigma_\alpha$), while a linear growth of intensity is predicted in the opposite case. These predictions hold even when the relative frequency shift between the gain/loss and coupling profiles is taken into account. The results presented here represent a very promising prediction of $\mathcal{PT}$-symmetric breaking using a manufacturable dual-core optical fiber. This breakthrough has significant potential for several applications, including all-optical switching and the development of robust high-power lasers.

Funding. Ministry of Education and Training (B2022- BKA-14); Narodowe Centrum Nauki (2019/33/N/ST7/03142, PRELUDIUM-17, UMO-2022/46/A/ST7/00238, MAESTRO-14).

Disclosures. The authors declare no conflicts of interest.

Optics EXPRESS

Data Availability. Data underlying the results presented in this paper are not publicly available at this time but may be obtained from the authors upon reasonable request.

References

1. C. M. Bender and S. Boettcher, "Real spectra in non-hermitian hamiltonians having $\mathcal{PT}$ symmetry," Phys. Rev. Lett. **80**(24), 5243–5246 (1998).
2. A. Mostafazadeh, "Exact $\mathcal{PT}$-symmetry is equivalent to hermiticity," J. Phys. A: Math. Gen. **36**(25), 7081–7091 (2003).
3. C. M. Bender, P. E. Dorey, A. F. C. Dunning, *et al.*, *Basics of $\mathcal{PT}$ Symmetry* (World Scientific, 2019), chap. Chapter 1, pp. 3–38.
4. C. Hang, G. Huang, and V. V. Konotop, "$\mathcal{PT}$ symmetry with a system of three-level atoms," Phys. Rev. Lett. **110**(8), 083604 (2013).
5. C. M. Bender, B. K. Berntson, D. Parker, *et al.*, "Observation of $\mathcal{PT}$ phase transition in a simple mechanical system," Am. J. Phys. **81**(3), 173–179 (2013).
6. J. Schindler, A. Li, M. C. Zheng, *et al.*, "Experimental study of active lrc circuits with $\mathcal{PT}$ symmetries," Phys. Rev. A **84**(4), 040101 (2011).
7. V. V. Konotop, J. Yang, and D. A. Zezyulin, "Nonlinear waves in $\mathcal{PT}$-symmetric systems," Rev. Mod. Phys. **88**(3), 035002 (2016).
8. A. Ruschhaupt, F. Delgado, and J. G. Muga, "Physical realization of -symmetric potential scattering in a planar slab waveguide," J. Phys. A: Math. Gen. **38**(9), L171–L176 (2005).
9. L. Luo, J. Luo, H. Chu, *et al.*, "Pseudo-hermitian systems constructed by transformation optics with robustly balanced loss and gain," Adv. Photonics Res. **2**(2), 2000081 (2021).
10. A. Mostafazadeh, "Pseudo-hermiticity versus pt symmetry: The necessary condition for the reality of the spectrum of a non-hermitian hamiltonian," J. Math. Phys. **43**(1), 205–214 (2002).
11. A. A. Zyablovsky, A. P. Vinogradov, A. A. Pukhov, *et al.*, "Pt-symmetry in optics," Phys.-Usp. **57**(11), 1063–1082 (2014).
12. K. Li, D. A. Zezyulin, P. G. Kevrekidis, *et al.*, "$\mathcal{PT}$-symmetric coupler with $\chi^{(2)}$ nonlinearity," Phys. Rev. A **88**(5), 053820 (2013).
13. Z. Lin, H. Ramezani, T. Eichelkraut, *et al.*, "Unidirectional invisibility induced by $\mathcal{PT}$-symmetric periodic structures," Phys. Rev. Lett. **106**(21), 213901 (2011).
14. A. Regensburger, C. Bersch, M. Miri, *et al.*, "Parity–time synthetic photonic lattices," Nature **488**(7410), 167–171 (2012).
15. A. U. Hassan, H. Hodaei, M.-A. Miri, *et al.*, "Nonlinear reversal of the $\mathcal{PT}$-symmetric phase transition in a system of coupled semiconductor microring resonators," Phys. Rev. A **92**(6), 063807 (2015).
16. H. Benisty, A. Degiron, A. Lupu, *et al.*, "Implementation of pt symmetric devices using plasmonics: principle and applications," Opt. Express **19**(19), 18004–18019 (2011).
17. E. Şeker, B. Olyaeefar, K. Dadashi, *et al.*, "Single-mode quasi pt-symmetric laser with high power emission," Light: Sci. Appl. **12**(1), 149 (2023).
18. A. Guo, G. J. Salamo, D. Duchesne, *et al.*, "Observation of $\mathcal{PT}$-symmetry breaking in complex optical potentials," Phys. Rev. Lett. **103**(9), 093902 (2009).
19. C. E. Rüter, K. G. Makris, R. El-Ganainy, *et al.*, "Observation of parity–time symmetry in optics," Nat. Phys. **6**(3), 192–195 (2010).
20. A. A. Sukhorukov, Z. Xu, and Y. S. Kivshar, "Nonlinear suppression of time reversals in $\mathcal{PT}$-symmetric optical couplers," Phys. Rev. A **82**(4), 043818 (2010).
21. R. El-Ganainy, K. G. Makris, D. N. Christodoulides, *et al.*, "Theory of coupled optical $\mathcal{PT}$-symmetric structures," Opt. Lett. **32**(17), 2632–2634 (2007).
22. S. Klaiman, U. Günther, and N. Moiseyev, "Visualization of branch points in $\mathcal{PT}$-symmetric waveguides," Phys. Rev. Lett. **101**(8), 080402 (2008).
23. A. Govindarajan, A. K. Sarma, and M. Lakshmanan, "Tailoring $\mathcal{PT}$-symmetric soliton switch," Opt. Lett. **44**(3), 663–666 (2019).
24. Y. Chen, A. Snyder, and D. Payne, "Twin core nonlinear couplers with gain and loss," IEEE J. Quantum Electron. **28**(1), 239–245 (1992).
25. N. V. Alexeeva, I. V. Barashenkov, A. A. Sukhorukov, *et al.*, "Optical solitons in $\mathcal{PT}$-symmetric nonlinear couplers with gain and loss," Phys. Rev. A **85**(6), 063837 (2012).
26. Y. V. Bludov, V. V. Konotop, and B. A. Malomed, "Stable dark solitons in $\mathcal{PT}$-symmetric dual-core waveguides," Phys. Rev. A **87**(1), 013816 (2013).
27. H. Ramezani, T. Kottos, R. El-Ganainy, *et al.*, "Unidirectional nonlinear $\mathcal{PT}$-symmetric optical structures," Phys. Rev. A **82**(4), 043803 (2010).
28. A. Sahoo, D. K. Mahato, A. Govindarajan, *et al.*, "Bistable soliton switching dynamics in a $\mathcal{PT}$-symmetric coupler with saturable nonlinearity," Phys. Rev. A **105**(6), 063503 (2022).
29. A. Sahoo, D. K. Mahato, A. Govindarajan, *et al.*, "Switching dynamics of femtosecond solitons in parity-time-symmetric coupled optical waveguides," Phys. Rev. A **106**(4), 043502 (2022).

Optics EXPRESS

30. X. Zhang, V. A. Vysloukh, Y. V. Kartashov, *et al.*, "$\mathcal{PT}$ symmetry in nonlinear twisted multicore fibers," Opt. Lett. **42**(15), 2972–2975 (2017).
31. R. Stępień, M. Franczyk, D. Pysz, *et al.*, "Ytterbium-phosphate glass for microstructured fiber laser," Materials **7**(6), 4723–4738 (2014).
32. M. Franczyk, D. Pysz, P. Pucko, *et al.*, "Yb^{3+} doped silica nanostructured core fiber laser," Opt. Express **27**(24), 35108–35119 (2019).
33. M. Franczyk, R. Stepien, D. Pysz, *et al.*, "Phosphate yb^{3+} photonic crystal fiber single-mode laser with enormous high pump absorption," Laser Phys. Lett. **11**(8), 085104 (2014).
34. J. Cimek, N. Liaros, S. Couris, *et al.*, "Experimental investigation of the nonlinear refractive index of various soft glasses dedicated for development of nonlinear photonic crystal fibers," Opt. Mater. Express **7**(10), 3471–3483 (2017).
35. R. Adair, L. L. Chase, and S. A. Payne, "Nonlinear refractive index of optical crystals," Phys. Rev. B **39**(5), 3337–3350 (1989).
36. P. Stajanca and I. Bugar, "Nonlinear ultrafast switching based on soliton self-trapping in dual-core photonic crystal fibre," Laser Phys. Lett. **13**(11), 116201 (2016).
37. M. Longobucco, P. Stajanča, L. Čurilla, *et al.*, "Applicable ultrafast all-optical switching by soliton self-trapping in high index contrast dual-core fibre," Laser Phys. Lett. **17**(2), 025102 (2020).
38. M. Longobucco, J. Cimek, L. Čurilla, *et al.*, "All-optical switching based on soliton self-trapping in dual-core high-contrast optical fibre," Opt. Fiber Technol. **51**, 48–58 (2019).
39. G. P. Agrawal, "Chapter 2 - fiber couplers," in *Applications of Nonlinear Fiber Optics (Second Edition)*, G. P. Agrawal, ed. (Academic Press, Burlington, 2008), pp. 54–99, second edition ed.